Assessing landscape dust emission potential using combined ground-based measurements and remote sensing data

J.R.C. von Holdt[1]; F.D. Eckardt[2]; M.C. Baddock[3] and G.F.S. Wiggs[4]

[1]Department of Chemical Engineering, University of Cape Town, Private Bag X3, Rondebosch, Cape Town 7701, South Africa

[2]Department of Environmental and Geographical Science, University of Cape Town, Private Bag X3, Rondebosch, Cape Town 7701, South Africa

[3]Geography and Environment, Loughborough University, Loughborough, Leicestershire, UK LE11 3TU

[4]School of Geography and the Environment, Oxford University Centre for the Environment, University of Oxford, Oxford, UK OX1 3QY

Corresponding author: J R C von Holdt (Johanna.vonholdt@uct.ac.za)

Key points:

- The combination of remote sensing and ground-based measurement is potent for studying dust emission potential across spatial scales
- Results demonstrate substantial variability of emission at each scale of analysis (individual erosional surface, landform, and landscape)
- A Boosted Regression Tree model determines the relative influence of specific variables controlling surface erodibility

Abstract

Modeled estimates of aeolian dust emission can vary by an order of magnitude due to the spatiotemporal heterogeneity of emissions. To better constrain location and magnitude of emissions, a surface erodibility factor is typically employed in models. Several landscape-scale schemes representing surface dust-emission potential for use in models have recently been proposed, but validation of such schemes has only been attempted indirectly with medium-resolution remote sensing of mineral aerosol loadings and high-resolution land-surface mapping. In this study, we used dust-emission source points identified in Namibia with Landsat imagery together with field-based dust-emission measurements using a Portable In-situ Wind Erosion Laboratory (PI-SWERL) wind tunnel to assess the performance of schemes aiming to represent erodibility in global dust-cycle modeling. From analyses of the surface and samples taken at the time of wind tunnel testing, a Boosted Regression Tree analysis identified the significant factors controlling erodibility based on PI-SWERL dust flux measurements and various surface characteristics, such as soil moisture, particle size, crusting degree and mineralogy. Despite recent attention to improving the characterisation of surface dust-emission potential, our assessment indicates a high level of variability in the measured fluxes within similar geomorphologic classes. This variability poses challenges to dust modelling attempts based on geomorphology and/or spectral-defined classes. Our approach using high-resolution identification of dust sources to guide ground-based testing of emissivity offers a valuable means to help constrain and validate dust-emission schemes. Detailed determination of the relative strength of factors controlling emission can provide further improvement to regional and global dust-cycle modeling.

Plain Language Summary

Atmospheric mineral dust plays an important role in Earth system processes, influencing climate, providing nutrients to ecosystems and affecting human health. The effect that atmospheric dust has on the climate and environment requires accurate modeling of emission at source, transport through the atmosphere, and deposition. To enable regional to global modeling of the dust cycle, therefore, requires realistic representation of where and when dust emission takes place. However, the highly variable nature of dust emission has resulted in modeling attempts producing disparate results. This research used Landsat remote sensing data in Namibia to identify sources of dust emission at high-resolution, followed by ground-based testing using a portable wind tunnel to assess surface classification schemes intended to

represent the surface in dust-emission models. Despite the proposed schemes offering valuable approaches for characterization of the land surface for modeling, globally applicable representation of dust emission is still hampered by the variability of small-scale emissions. At the sub-landform level of our analysis, the heterogeneous nature of dust emission results from the highly variable nature of the surfaces. Our analysis identified several factors controlling the potential for surfaces to emit dust that can be used as inputs to improve dust modeling.

1 Introduction

Wind-driven processes of sediment transport are important in the Earth system and consequently have been the focus of many modeling attempts (Ravi et al., 2011; Shao et al., 2011). The dynamics of mineral dust emission are fundamentally controlled by a combination of the power of the wind to erode (erosivity) and the resistance of an emitting surface to erosion (erodibility) (Webb & Strong, 2011). Interactions between erosive and resisting forces are complex and result in dust emission being spatially and temporally highly heterogeneous (e.g. Bryant et al., 2007; Gillette, 1999; Gillies, 2013; Mahowald et al., 2003; Taramelli et al., 2013). Improvements in dust-emission modeling remains an important contemporary research goal since existing models have a limited capacity to accurately account for the spatiotemporal variability of dust emission within dust sources (Haustein et al., 2015; Parajuli et al., 2014; Shao et al., 2011).

Modeling of dust emission must account for factors that affect the threshold friction velocity (u_{*t}), and as a result, the variable erodibility of the surface (Marticorena & Bergametti, 1995, Shao et al., 1996). Some of the major drivers influencing the variability of the surface erosion thresholds include soil moisture (influenced by relative humidity), particle size, degree of crusting (including physical, saline and biological soil crusts), and mineralogy of surface sediments (e.g. Belnap & Gillette, 1998; Buck et al., 2011; Cornelis et al., 2004; Gillette et al., 1982; King et al., 2011; Marticorena & Bergametti, 1995; McKenna Neuman & Nickling, 1989; McKenna Neuman & Maxwell, 2002; Munkhtsetseg et al., 2016; Sweeney et al., 2016), as well as surface roughness (characterized by the aerodynamic roughness length, z_o) (Raupach et al. 1993), with vegetative and topographic (micro to macro) roughness having significant influences (e.g. Gillies et al., 2006; Okin & Gillette, 2001; Sankey et al., 2010). Incorporating the influence of these surface characteristics into soil erodibility and dust emission predictions is one of the biggest challenges for dust simulation, especially given that global data sets of

these input variables are not always available, or are not at a spatial scale appropriate for model input.

A surface erodibility factor is typically used in dust models to constrain the observed spatial heterogeneity of emissions (Zender et al., 2003). Several dust-emission mapping schemes at the landscape scale have attempted to account for erodibility as a regulator of emission potential for use in dust models (e.g. Ashpole & Washington, 2013; Baddock et al., 2016; Bullard et al., 2011; Parajuli et al., 2014; Parajuli & Zender, 2017). The erodibility factor has typically been based on various physical assumptions of the influence of geomorphology, topography and hydrology on dust emission (Ginoux et al., 2001; Zender et al., 2003). Alternatively, empirical approaches based on satellite-derived data, including surface reflectance (e.g. Grini et al., 2005) have also been formulated. Bullard et al. (2011) and Parajuli et al. (2014) presented high resolution land-surface classifications based on the potential emissivity of specific geomorphic types and land covers. A recent global characterization of dust-emission potential by Parajuli & Zender (2017), the Sediment Supply Map (SSM), combines drainage area (a proxy for long-term hydrologic transport and deposition of sediment) with empirically-derived surface reflectance from the Moderate Resolution Imaging Spectroradiometer (MODIS) blue channel. The combination of these datasets encapsulates two important aspects of sediment supply, namely the accumulation of fine sediments in basins as a supply of dust-sized material, and the reflectance of different land surface types based on their surface sediment supply potential (Parajuli & Zender, 2017). The SSM is a landscape-scale (~500 m) erodibility map that provides numerical estimates of dust emission potential for use in global dust-cycle models.

While such classifications are produced at a high spatial resolution relative to current dust modeling approaches (Shi et al., 2016; Parajuli & Zender, 2017), it is recognised that a range of influences affecting dust emission operate at scales below the landscape scale. As such, the scale at which dust-emission processes are investigated has a marked influence on the spatial representation of emission variability. Webb & Strong (2011) highlight this by proposing that wind erosion drivers can be understood at a range of scales, with different influences apparent at successive scales of analysis: grain to surface ($<10^0$m), landform ($\sim10^1$ - 10^2m), landscape ($\sim10^3$m), and regional to global scales ($>10^4$m). Recent landscape-scale dust-emission mapping schemes have not yet been assessed rigorously by ground-truthing and uncertainty remains regarding how well these surface classifications account for the potential variability in emission known to exist at the landform and sub-landform scales (Sweeney et al., 2011).

Our understanding of dust-emission processes has been greatly enhanced by studies that have identified dust sources on global, regional and landscape scales through various remote sensing approaches primarily using the Total Ozone Mapping (TOMS) and more recently the MODIS sensors (e.g. Baddock et al., 2016; Bullard et al., 2008, Ginoux et al., 2012; Huang et al., 2007, Lee et al, 2012, O'Loingsigh et al., 2015; Prospero et al., 2002; Schepanski et al., 2007, 2012; Vickery et al., 2013; Washington et al., 2003). However, a fuller appreciation of the smaller-scale controls contributing to the variability in dust emission also depends on the improved characterisation of dust sources at a sub-landform scale. Ground-based studies are crucial, because the sub-landform variability of emission from dust producing surfaces has proven difficult to investigate using other means. However, using ground-based measurements to validate predictions of dust emission potential (such as that provided by the SSM) remains a challenge, because of the disconnect between process studies and flux measurements, necessarily performed at a landform to sub-landform scale, *versus* the regional or global focus taken by modeling studies. This is partly due to the limitation posed by a relatively coarse spatial resolution in remote sensing together with a lack of dedicated field studies quantifying sub-landform variability (Haustein et al., 2015). Small-scale studies allow quantification of dust emission from specific landforms and the combination of surfaces within these landforms. The advantage of a high-resolution approach to dust source-point identification has recently been demonstrated by von Holdt et al. (2017) who used Landsat imagery covering a 25-year period to identify the landform-scale dust sources in the Namib Desert of southern Africa.

The increased spatial resolution of Landsat (15-30 m) compared to other remote sensing data used to date (e.g. MODIS 250-1000 m) has improved accuracy for dust source-point identification, allowing the study of dust emission at landform scales and guiding field measurement at the sub-landform scale (von Holdt et al., 2017). The spatial variability of dust emission at sub-landform scale has been investigated by several studies using a PI-SWERL wind tunnel (Etyemezian et al., 2007) to measure the dust emission potential of surfaces from a variety of landforms found in desert regions (e.g. Bacon et al., 2011; King et al., 2011; Sweeney et al., 2011; 2016). The small size and portable nature of this instrument allows for replicate testing of multiple surfaces in locations that would not be accessible by conventional, larger footprint wind tunnels. Furthermore, given the size of the PI-SWERL (0.57 m diameter), its measurements are at a spatial scale corresponding to the grain and surface scale controls on dust emission ($<10^0$ m) (Webb and Strong, 2011). Using a Landsat analysis to guide in situ measurements for quantifying surface- to landscape-scale variability of dust emission (von

Holdt et al., 2017), offers a means for testing dust-emission schemes and improving how surface erodibility is characterized in dust modeling.

This study aims to use a portable wind tunnel to estimate relative emissivity from different land surface types, doing so within the context of recently proposed methods for classifying surface emission potential for dust modeling efforts. Assessment of measured dust fluxes from classified surfaces is used to contribute a novel test of these new schemes and more broadly, inform regional and global dust models. For flux measurements,field-based emission sampling with a PI-SWERL was guided by using high a resolution, Landsat-derived, dust source point inventory created for the Namib Desert (von Holdt et al., 2017). This approach allows assessment of emission variability across a range of spatial scales by combining PI-SWERL point measurements with landform classification. The secondary objective was to examine the emission measurements and a range of surface properties (soil moisture, degree of crusting, particle size and mineralogy) using a Boosted Regression Tree (BRT) analysis to determine the most significant erodibility factors for the dust source points.

2 Regional setting and field sites

The Namib Desert is one of the major southern African dust sources (Vickery et al., 2013; von Holdt et al., 2017), and is appreciable at the hemispheric scale (Ginoux et al., 2012). This region comprises several desert landforms, including 12 westward-flowing ephemeral rivers, numerous small inland playas and large coastal sabkhas, sand deposits which include sand sheets and sand dunes; and extensive areas of stony desert comprising gravel stone pavements dissected by non-fluvial ephemeral drainage channels (Bullard et al., 2011; Jacobsen et al., 1995; Goudie & Viles, 2015). Dust emission from the Namib Desert has been mostly associated with the terminal stages of the dry river valleys and coastal sabkhas and inland playas (Dansie et al., 2018; Eckardt & Kuring, 2005; Vickery & Eckardt, 2013; von Holdt et al., 2017). The Kuiseb, Huab and Omaruru rivers were identified as the most emissive river systems based on MODIS true colour imagery analysis from 2005 to 2015, whereas Conception Bay and the Ugab Pans were the most emissive sabkhas (von Holdt et al., 2017) (Figure 1 a). The present study uses PI-SWERL measurements to assess dust emission potential predicted from classification schemes applied to the three most emissive catchments determined by von Holdt et al. (2017), in addition to the Ugab sabkha system (marked U in Figure 1a). The PI-SWERL measurements from von Holdt et al. (2017) are a subset of the data used in the present paper (40% of the total data set, Table S1), and while von Holdt et al. (2017) examined the river

systems on a case-by-case basis, the current investigation examines dust emission across multiple scales (erosional surface, landform, and landscape) for the Namib Desert study area.

3 Methods

3.1 Geomorphology and dust emission scheme mapping

Geomorphological units were mapped in the study area following the land-surface classification based on geomorphology used by Bullard et al. (2011) in their Preferential Dust Scheme (PDS) (see also Baddock et al., 2016). The PDS classes included lake systems, including dry and ephemeral lakes (playa and sabkha pans), alluvial systems (high- and low-relief), stony systems (including stone pavements intersected by ephemeral drainage channels), aeolian systems (sand sheets and dunes), loess and low emission surfaces, such as bedrock. The Namib loess deposits consist predominantly of fluvially reworked loess in the ephemeral river valleys (Eitel et al., 2001) and were mapped as part of alluvial systems as they are not distinguishable at the scale of mapping used in the present study. The study area mapped consisted of the Landsat tiles analysed by von Holdt et al. (2017) (Figure 1 a) and used a combination of remote sensing data, 1:250 000 geological maps from the Geological Survey of the Ministry of Mines and Energy of Namibia and field observations. The remote sensing data included Google Earth images, Landsat 8 false colour imagery (bands 7,5,3) and the Shuttle Radar Topography Mission (SRTM) 30-m digital elevation model to distinguish between low- and high-relief, as well as degree of incision of alluvial systems. The 2289 dust source points identified with the aid of Landsat imagery between 1990 and 2016 by von Holdt et al. (2017 were classified according to the PDS land-surface classes at a landscape scale. Mapping was done in QGIS v 2.18.12 (QGIS development team, 2016).

The Land Surface Map (LSM) and Sediment Supply Map (SSM) were made available as rasters by Parajuli & Zender (2017). The LSM (Parajuli et al., 2014) was originally developed by mapping the Middle East and North Africa region according to 12 spectral land cover classes with high-resolution Google Earth Pro images and polygons created as training samples for a global supervised classification which used the maximum likelihood method in ArcGIS, as applied to the global Blue Marble (MODIS RGB) image mosaic. To enable better comparison of the PDS and LSM outputs, the Parajuli et al. (2014) spectral land cover classes were reclassified according to the geomorphology based PDS land-surface classes (Bullard et al., 2011). The LSM is used for a qualitative and quantitative comparison with the SSM produced

globally by Parajuli & Zender (2017). The original LSM land cover classes used in Parajuli et al. (2014) are included in the Supporting Information Figure S1.

The SSM is derived through a combination of the upstream catchment area and the surface reflectance captured in the blue band (459-479 nm) from the same Blue Marble mosaic used for determination of the LSM. The upstream catchment size is suggested to provide an estimate of the transport and deposition of sediments and highlights areas of sediment accumulation, whereas the reflectance serves as a proxy for highly erodible surfaces such as playas and dunes. The value for the SSM is based on a scale from 0 – 1, with the Bodélé Depression in Chad regarded as the most emissive source with a maximum value of 1 (Parajuli & Zender, 2017).

3.2 PI-SWERL dust-emission measurements

Dust-emission measurements from the PI-SWERL instrument were used to measure the potential for dust flux from different desert surfaces, with the PI-SWERL now being a widely used technique (e.g., Bacon et al., 2011; Etyemezian et al., 2007; Goossens & Buck, 2009; Sweeney et al., 2008, 2011). The specific methodology and test parameters for the PI-SWERL are presented in von Holdt et al. (2017). The dust emission flux (E_f, mg m^{-2} s^{-1}) was calculated using the following equation from Sweeney et al. (2011):

$$E_f = \frac{\sum_{begin,i}^{end,i} C \; x \; F}{(t_{end,i} - t_{begin,i}) \cdot A_{eff}}, \qquad (1)$$

where C is the dust concentration (mg m^{-3}) of PM_{10} (Particulate matter <10 μm) , F is the flow rate of air through the chamber (L s^{-1}), A_{eff} is the test area underneath the PI-SWERL annular ring (m^2), and t is the time (s) at the beginning (t_{begin}, i) and end (t_{end}, i) of the RPM step test level, i (Sweeney et al., 2011). In order to take measurements at sites of known dust emission, the PI-SWERL was deployed at a total of 17 sites identified from Landsat (von Holdt et al., 2017) (Figure 1 a). A further three sites were tested representing low emission surfaces, i.e. the gravel pavements within stony systems and sand dunes within aeolian systems. These non-emissive sites were included in the study to obtain the full range of emission potential and for purposes of the regression analysis. The stone pavements chosen as test sites were selected based on the presence of a vesicular A soil horizon (Av) (McFadden, 2013, Sweeney et al., 2013) as these horizons are indicators of dust activity, predominantly as inputs to soils.

At each site a 10 m tape marked at 1 m intervals was laid out as close as possible to the co-ordinates of emission source points determined from Landsat. For consistency, transects were

all laid out perpendicular to the direction of the north-east regional wind (the Bergwind) that is responsible for much of the large-scale dust emission in the Namib (Vickery & Eckhardt, 2013). All 17 sites underwent visual confirmation on the ground of the surfaces identified as potentially emissive. The site was assessed, and a final *in situ* decision was made regarding the placement of the transect so as to include all the different surface types that were apparent locally. At each location of testing, 3 to 10 individual runs were made at metre intervals along a 10 m linear transect with the number of test runs dependent on the homogeneity of the surfaces within the transect and variability of the emission flux results.

A further decision regarding the number of runs to perform was made based on the PI-SWERL results at the time of testing. Floodplain terraces present within alluvial systems composed of silt crusts with variable amounts of sand for saltation and nebkhas situated on the terraces as well as loose erodible material present in between the silt crusts proved to be highly variable and as a result, 10 transects were done on these terraces. In contrast, sand dunes within the aeolian systems were relatively uniform in emission potential and so fewer measurements were carried out on these surfaces and were largely for exploratory purposes (Table 1). Dune sand deposits have not been identified as significant point source emitters from Landsat but have been identified as low intensity dust sources covering large areas and hence a potentially appreciable source of dust (Bullard et al., 2004; Crouvi et al., 2008; Strong et al., 2010).

The PI-SWERL measurements were classified according to the individual erosional surfaces that were being tested. The individual surfaces were then aggregated first to a landform scale and lastly to a landscape scale (Table 1). Details of the PI-SWERL test sites and landform classifications are given in Table S1 of the Supporting Information. We used a mixed effects model to investigate the relationship of dust emission potential within each spatial scale (suited to unbalanced replicates) with catchment identity set as a random effect (as in Sankey et al., 2011) followed by an analysis of variance for the fixed-effects terms (Table 1 categories for Landscape, Landform and Surface respectively). Data at all scales were log-transformed before model runs to satisfy the assumption of the normality of the residuals. All models and significance testing were performed in R 3.4.1 (R Development Core Team, 2017) using the '*nlme*' package (Pinheiro et al., 2018). A threshold p-value of <0.05 was regarded as significant. A determination of spatial autocorrelation using the Moran's I test statistic was performed with the '*ape*' package (Paradis & Schliep, 2018) in R 3.4.1. at all spatial scales.

Table 1 Breakdown of the categories of geomorphology considered in the statistical analysis[a]

278

SURFACE ($<10^{-1}$ m) (*n*=individual PI-SWERL measurements) *n*=128	Loose Erodible Material (LEM) (25)	Crust: high saltators (22)	Crust: medium saltators (12)	Crust: no saltators (31)	Low % gravel (17)	High % gravel (9)	Salt crust: with and without saltators (12)
LANDFORM (10^1-10^2m) (*n*=PI-SWERL transects) *n*=17	Active channel (1) Terraces (10)		Drainage channel (2) Pavement (4)			*	*
LANDSCAPE (10^3 m) (*n*=landforms sampled) *n*=12	Alluvial systems (5)		Stony systems (4)			Aeolian systems (1)	Ephemeral lake systems (2)
CATCHMENT	Kuiseb, Omararu, Huab, Ugab						

279 [a] Increasing spatial scale of enquiry moving down the table. Catchment was set as random
280 effect across the Namib Desert study region. 'Aeolian systems' and 'Ephemeral lake systems'
281 landscapes were not analysed at Landform scale due to insufficient number of sample points
282 and sampling conditions.

283

284 3.3 Characterization of surface properties and Boosted Regression Tree (BRT) analysis

285 A BRT model was used to identify the most relevant variables that controlled surface
286 erodibility using the surface properties at each PI-SWERL field testing site. This analysis was
287 performed following Elith et al. (2008) using the '*dismo'* package (Hijmans et al., 2016) in R
288 with a learning rate of 0.005 and a tree complexity of 5. E_f (Equation 1), representing the overall
289 surface erodibility, was used as the response variable and specific predictor variables included
290 compressive and shear strength to quantify the degree of crusting, soil moisture content,
291 particle size and elemental composition to assess the influence of mineralogy. For those
292 properties tested in the laboratory, one surface sample was taken with a flat spade to a depth of

0.02 m directly next to each PI-SWERL run at the time of testing. Further details of the BRT analysis are given in Section S1 of the Supporting Information.

The degree of consolidation or crusting of the surface was assessed in the field by measuring the compressive and shear strength of the surface. Unconfined compressive strength was measured on the test surface at each PI-SWERL run site using a Pocket Soil Penetrometer H-4195 and shear strength using a Torvane H-4212 pocket shear vane (Humboldt Mfg. Co., Illinois, USA). At each site a minimum of three measurements of both compressive and shear strength of the surface were taken. If a large difference in individual measurements was encountered, additional measurements were taken to increase representativeness of measurement.

The near-surface volumetric soil moisture content at the time of PI-SWERL sampling was measured in the field with a Delta-T Devices ML3 ThetaProbe soil moisture sensor. A minimum of three measurements were taken at each PI-SWERL measurement site by inserting the probe to just below the soil surface. We note that the probe was designed to be fully inserted into the soil medium (to a depth of 0.06 m), producing values for a deeper soil volume. Our non-standard application of the instrument (not inserting it fully into the soil) is intended to provide a relative measure of near-surface soil moisture, but has not been vetted through further gravimetric measurements. The ThetaProbe was therefore inserted only into the top 0.02 m. For this study, establishing a gauge of soil moisture as close as possible to the surface (which has a strong influence on erosion potential (Wiggs et al., 2004) outweighed specific quantification of soil moisture level.

For particle size analysis, all the samples were air dried at 25°C to a constant weight and sieved to 1 mm. The >1 mm split was further sieved to determine the coarse sand and gravel fractions. The <1 mm split was used to determine the particle size distribution by laser diffraction using a Malvern Mastersizer 2000 attached to a Hydro 2000G dispersion unit. The samples were cone and quartered to obtain a representative sample and placed in a tap water solution overnight, shaken for half an hour and again for half an hour the next day before introduction to the dispersion unit and further sonicated for 180 seconds prior to measurement. Particle size statistics including texture classes, modes, kurtosis, skewness and sorting were calculated using Gradistat software (Blott & Pye, 2001).

The gravel concentration in the surface sediments determined by sieve analysis served as a proxy for gravel-cover density. These results were confirmed by an unsupervised classification

of a photograph of each surface with a gravel cover performed in Erdas Imagine 2015-2016 (Leica Geosystems, Atlanta, Georgia, USA). Gravel cover densities of <30% were classified as low gravel cover and densities of >30% as high gravel cover. This distinction was chosen based on the analysis by Wang et al. (2012), who found that dust emission increases with increasing gravel cover up to a density of 30%, after which dust emission decreases.

Finally, milled samples of the <1 mm soil fraction were analyzed in the laboratory for Mg, Al, S, Cl, K, Ca, Ti, Mn and Fe. with a Spectroscout energy-dispersive X-ray Fluorescence (XRF) analyzer (SPECTRO Analytical Instruments, Kleve, Germany). The instrument was calibrated with a certified standard GBW07312 (National Research Centre for CRMs, Beijing, China) for which technical concentrations were obtained from NOAA Technical memorandum NOS ARCA 68 (1992).

4 Results

4.1 Dust emission scheme mapping and Landsat-derived dust source points

Stony systems and bedrock cover extensive areas of the Namib study area when mapped according to the PDS classification (Figure 1 b). Two extensive aeolian systems of the Namib Sand Sea in the south and the Skeleton Coast dunefield in the north account for the second largest portion of the land area. In the present study, the PDS classification was applied to the 2289 dust source points observed from Landsat imagery (1990-2016) by von Holdt et al. (2017) (Figure 1; Figure 2). Overall, the ephemeral lake systems and alluvial systems cover a very small proportion of the study area (2% of area) but contribute just over three-quarters of observed source points (77% of plumes) (Figure 2). In contrast, are stony systems (27% of area, 22% of source points) and aeolian systems (15% of area, 0.5% of source points), which cover large areas, but contain fewer point sources of dust emission. Additional details of the landform classification for the dust source points performed in the present study are given in section S2 of the Supporting Information.

The representation of the landscape according to the LSM (Figure 1 c) is noticeably different from the PDS, with large areas of bedrock and stony systems classified as either alluvial system or ephemeral lake. In addition, a large part of the Namib Sand Sea is classified as stony system, an issue noted by Parajuli & Zender (2017). Relatively small areas of a landscape are responsible for most of the dust emission (e.g. Bullard et al., 2008; Gillette, 1999; Lee et al., 2009) which is evident when assigning a level of dust emission potential to the PDS land

surface classification following Bullard et al. (2011) (Figure 1 d). Alluvial systems and ephemeral lake systems are the highest potential emitters, aeolian systems have low to medium dust emission potential and stony systems and bedrock are low potential emitters. The colours assigned to low, medium and high emission potential categories follow the colour scheme used in the SSM (Figure 1 e) by Parajuli & Zender (2017). The SSM highlights the elevated potential of alluvial systems to emit dust, but when mapped, results in a more extensive alluvial coverage than represented by the PDS scheme.

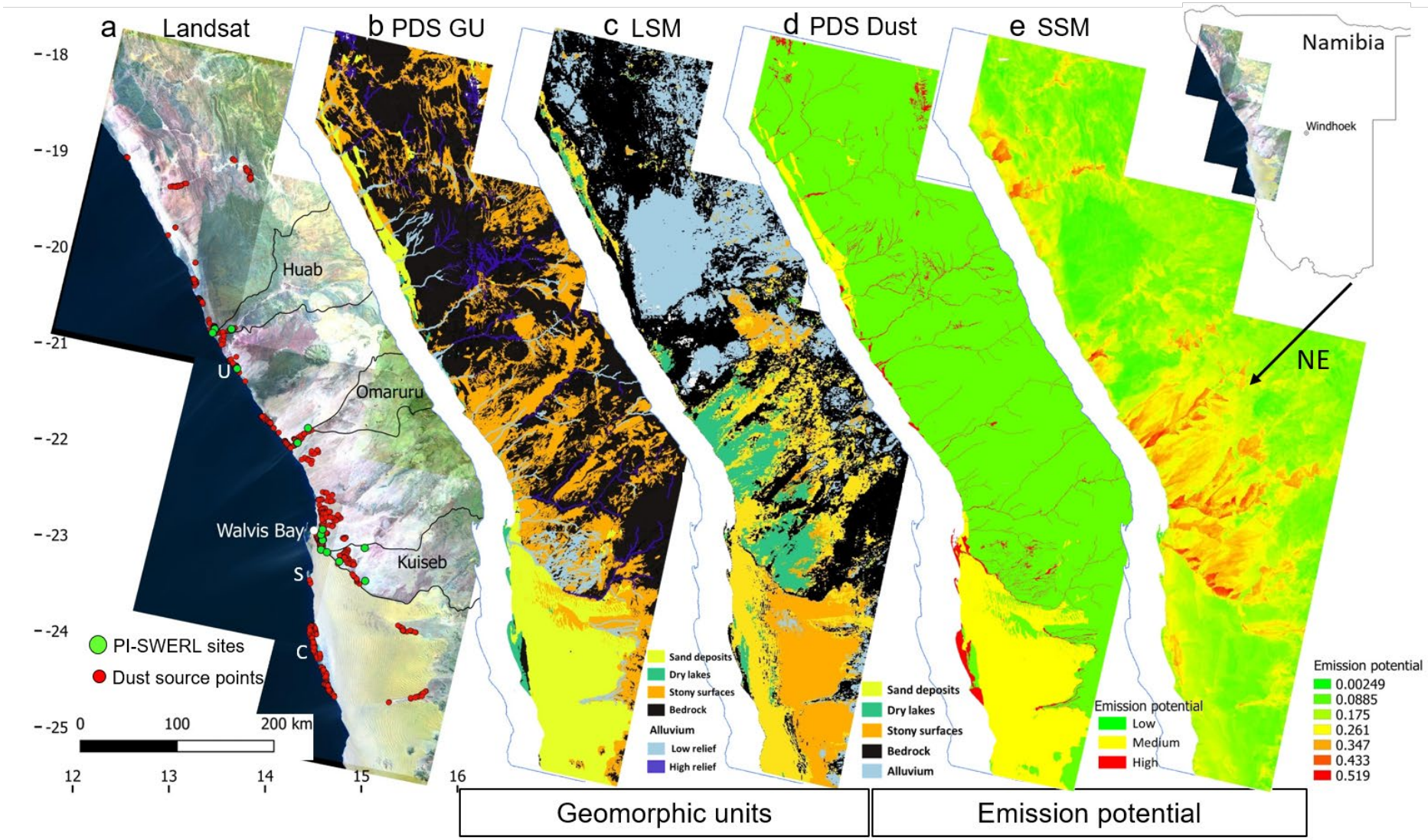
a Landsat
b PDS GU
c LSM
d PDS Dust
e SSM
Namibia
Windhoek
NE
Huab
Omaruru
Walvis Bay
Kuiseb
U
S
C
PI-SWERL sites
Dust source points
0 100 200 km
-18
-19
-20
-21
-22
-23
-24
-25
12
13
14
15
16
Sand deposits
Dry lakes
Stony surfaces
Bedrock
Alluvium
Low relief
High relief
Emission potential
Low
Medium
High
0.00249
0.0885
0.175
0.261
0.347
0.433
0.519
Geomorphic units
Emission potential

364

365

366 **Figure 1 Geomorphology and dust emission potential mapping of the Namib Desert area covered in this study. (a) Landsat false-colour image**
367 **showing the seven tiles included in the Landsat source point analysis, and the 2289 Landsat points from von Holdt et al. (2017), key river catchments**
368 **and PI-SWERL testing sites, (b) PDS GU geomorphic land surface classes per Bullard et al. (2011), (c) Land Surface Map (LSM) of Parajuli &**
369 **Zender (2017), (d) dust emission potential according to PDS emission categories (PDS Dust), (e) Sediment Supply Map (SSM) showing dust emission**
370 **potential based on surface reflectance on a unitless scale from 0 to 1 with the maximum value equated to the Bodélé Depression (Parajuli & Zender**
371 **(2017). In (a), U: Ugab pan complex, S: Sandwich Harbour, C: Conception Bay. Direction of predominant north easterly dust-producing winter**
372 **wind (Bergwind) is indicated by black arrow in (e).**

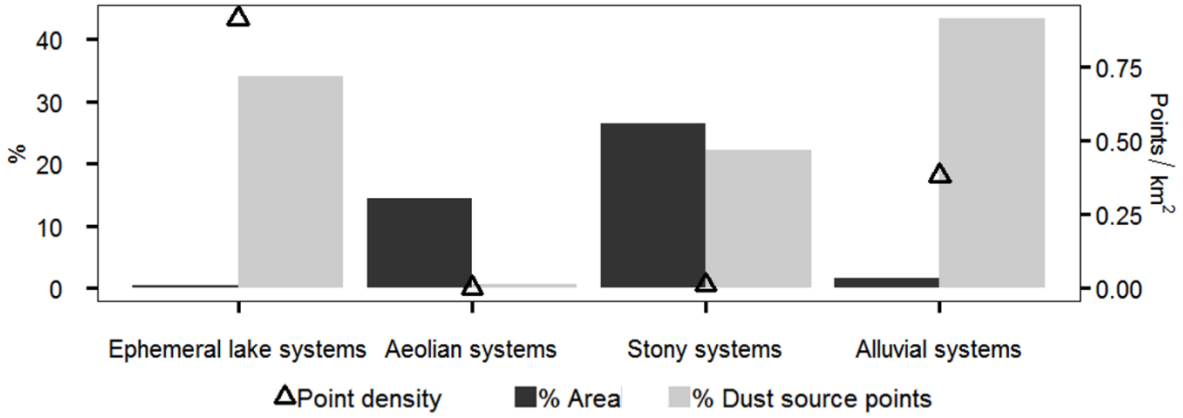

Figure 2 Areal extent of geomorphic landscape classes (% of total area) and frequency of dust source points within them (expressed as % of total number, as well as points per km^2) identified through Landsat analysis of the Namib Desert. Ephemeral lake systems (which include playa and sabkha pans) have the lowest extent within the study area (850 km^2), but show the highest density of source points. The stony systems have the highest areal coverage (45,000 km^2), but show a low density of source points. Alluvial systems have the highest number of source points overall (43%) but cover 4% of the study area. Aeolian systems cover 15% of the study area but were responsible for <1% of the source plumes identified.

4.2 Measured emission fluxes

The surface scale analysis of the PI-SWERL measurements illustrates the inherent variability of dust emission at a sub-landform scale (Figure 3). At this scale, the most emissive undisturbed surfaces occurred where loose erodible material (LEM) was present. The presence of such material was particularly associated with the presence of small nebkha dunes interspersed between crusted fluvial deposits within the valley fill terraces and within the drainage channels of the stony systems. In Figure 3, a distinction between the crusted surfaces present in the channels or on the terraces could be made based on the relative presence of saltators determined by inspection of the surface before a PI-SWERL test. Figure 3 indicates that LEM-dominated surfaces (geometric mean: 0.3188 mg m^{-2} s^{-1}) and those crusts with abundant sand for saltation (geometric mean: 0.342 mg m^{-2} s^{-1}) were significantly more emissive than the other surface types (p value < 0.001) (summary statistics in Table 2). Pavement surfaces with varying densities of gravel were found predominantly within the stony systems and in some river terraces. The low-density stone pavement (gravel cover <30%) was significantly more emissive (geometric mean: 0.02004 mg m^{-2} s^{-1}) than the surfaces with a high density of gravel cover (>30%). High density gravel surfaces (geometric mean: 0.0022 mg m^{-2} s^{-1}), crusts with no saltators (geometric mean: 0.0046 mg m^{-2} s^{-1}) and salt crusts (geometric mean: 0.0008 mg m^{-2} s^{-1}) were the lowest emitters. All p values for significance tests are reported in the Supporting Information Tables S3 to S5.

Aggregating the observed emission fluxes within the landscape scale classes found in dust emission potential schemes illustrates the problematic nature of representing sub-landform scale variability at a larger scale (Figure 4). The greatest amount of variability was present in the stony and alluvial systems and when aggregated to the landscape scale, the geometric means for these two classes were not significantly different (Figure 4 a). Notably, the lake systems are significantly different (p value = 0.040) and consistently showed low emissivity during the time they were tested (geometric mean: 0.0022 mg m^{-2} s^{-1}). The ephemeral lake systems tested included the Huab playa and Ugab sabkha (Figure 1 a), where significantly less dust was emitted than the other three geomorphic landscape units as quantified by the PI-SWERL (alluvial systems geometric mean: 0.0379 mg m^{-2} s^{-1} and stony systems geometric mean: 0.0102 mg m^{-2} s^{-1}). Aeolian systems were not included in the landscape-scale analysis due to insufficient sample size, but had a geometric mean of 0.0640 mg m^{-2} s^{-1} based on the individual PI-SWERL measurements (Table 2).

The variability in the alluvial and stony systems was further resolved by looking at distinct landforms present within these two broad landscape classes (Figure 4 b and c). In the case of the stony systems class, a fundamental distinction could be made between stone pavement surfaces dominated by the presence of coarse lag gravel, and portions of pavement where micro drainage channels (c. 0.1 m deep) were found (Figure 4 d and e). In turn, the low relief alluvial class could also be divided between portions of ephemerally active river channel and valley fill terraces, the latter situated above the channel (Thomas et al., 2017) (Figure 4 f and g). The river valley fill terraces (within alluvial systems) were on average the most emissive landform (geometric mean E_f: 0.0651 mg m^{-2} s^{-1}), followed by the stony systems exhibiting drainage channels (geometric mean: 0.0318 mg m^{-2} s^{-1}). The gravel pavements (geometric mean: 0.0075 mg m^{-2} s^{-1}) and active river channels (geometric mean: 0.0082 mg m^{-2} s^{-1}) were less emissive. In terms of statistical separation, however, only the stony pavements had a lower emission rate than the alluvial terraces (p-value = 0.00769).

The rapid, multi-replicate PI-SWERL testing allows the spatial variability in emission flux from a given surface, landform or landscape to be measured (King et al., 2011; Sweeney et al., 2011). The same crust within a 10 m transect can be largely non-emissive (0.003 mg $m^{-2}s^{-1}$) in the absence of available sand for saltation, but highly emissive (0.646 mg $m^{-2}s^{-1}$) where an abundant supply of saltators is present. Emission rates generated by the PI-SWERL testing of surfaces reflect the relative presence of only those saltators under the instrument footprint, resulting in non-emissive runs on crust where no saltators are present. However, river terraces surrounded by an abundant supply of sand will undergo widespread bombardment by saltation during a high friction velocity wind event. In such circumstances, it is possible that the entire transect will become highly emissive under the continued bombardment of the available saltators and stockpiles of LEM dispersed between the terraces. To test the degree to which individual measurements were spatially autocorrelated, a Moran's I test was performed for individual measurements within a transect and were not found to be spatially autocorrelated (for example p = 0.0705 using Moran's I for Huab transect 2 and p = 0.090 for Kuiseb 5) indicating that the sampling density was adequate, and autocorrelation is not relevant at the surface scale analysis. A higher sampling density is not possible given the size of the PI-SWERL.

4.3 Emission fluxes and relation to land surface classification schemes

The PI-SWERL provides a relative quantification of dust emission rates from the surface, against which the emission potential of different geomorphic classes in surface classification schemes (PDS, SSM/LSM) can be compared. Comparing the geometric mean of measured dust emission of the PI-SWERL transects across landforms against the SSM index values for the location of each PI-SWERL transect provides a means to assess and contextualise the SSM values (Figure 5). Also represented in Figure 5 is the land surface classification as per the PDS scheme by Bullard et al. (2011) and the LSM classification by Parajuli et al. (2014). Determination of the classification between the two different schemes differs considerably, for instance, with LSM classifying two out of the 20 transect locations as bedrock, while PDS identified them as either dry lake or alluvial systems (Figure 5). Elsewhere, LSM was found to classify PDS alluvial systems as bedrock with sediment and stony systems as Playa/Sabkha. The PI-SWERL results do not show a clear relationship between the measured dust emission and the SSM values. The SSM values for the entire study area range from a minimum of 0.002 to a maximum of 0.519 with a mean of 0.187, with the peak geometric mean transect emission rate (0.2191 mg m^{-2} s^{-1}) corresponding to a moderate SSM value (0.25) (Figure 5). Furthermore, a wide range of emissivity (0.002 to 0.2191 mg m^{-2} s^{-1}) is seen in the narrow range of SSM values between 0.23 to 0.27. This range covers the LSM categories of stabilised sand deposit, sand deposit on bedrock and bedrock, but is more appropriately classified as predominantly alluvial system and some stony system according to the PDS map. The highest SSM value for the PI-SWERL test sites was 0.46, which corresponded to a stony system with an emission value of 0.0127 mg m^{-2} s^{-1}. Other high SSM values (>0.3) mostly occurred within alluvial systems, with measured emission values varying widely between 0.008 and 0.12 mg m^{-2} s^{-1}, and the lowest emission flux value in this range associated with the active channels. The locations of the dust source points identified by von Holdt et al. (2017) with Landsat imagery in Figure 1 (a) have SSM values with a range of 0.078 to 0.508 and a mean of 0.245.

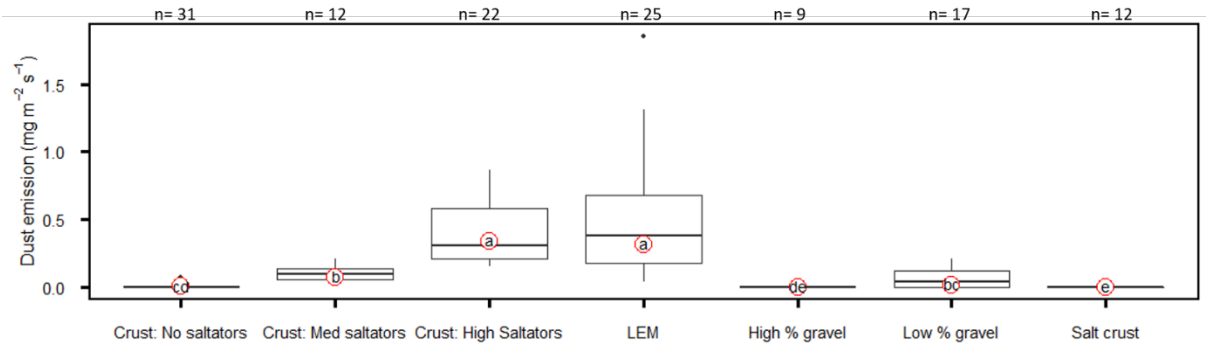

474

475 **Figure 3: Dust emissions from surface categories within all landscapes. The loose erodible**
476 **material (LEM) surface type consists of unconsolidated sediments and is found in ephemeral**
477 **drainage channels of stony systems and on terraces of alluvial systems between silt crusts and**
478 **nebkhas (Figure 4, left and right photos, respectively). The measurements carried out in the**
479 **aeolian system were also included in the LEM category. The crust surface class occurs in**
480 **alluvial systems and was subdivided based on abundance of sand available for saltation (none,**
481 **medium, high). Gravel surfaces found both in stony systems in pavements and alluvial systems**
482 **in terraces were subdivided based on the density of gravel cover (Low % with <30% gravel**
483 **cover and High % with > 30% gravel cover). Salt crusts were found within ephemeral lake**
484 **systems with and without saltators present. Letters indicate significant difference and are**
485 **plotted at the geometric mean of each surface category.**

486

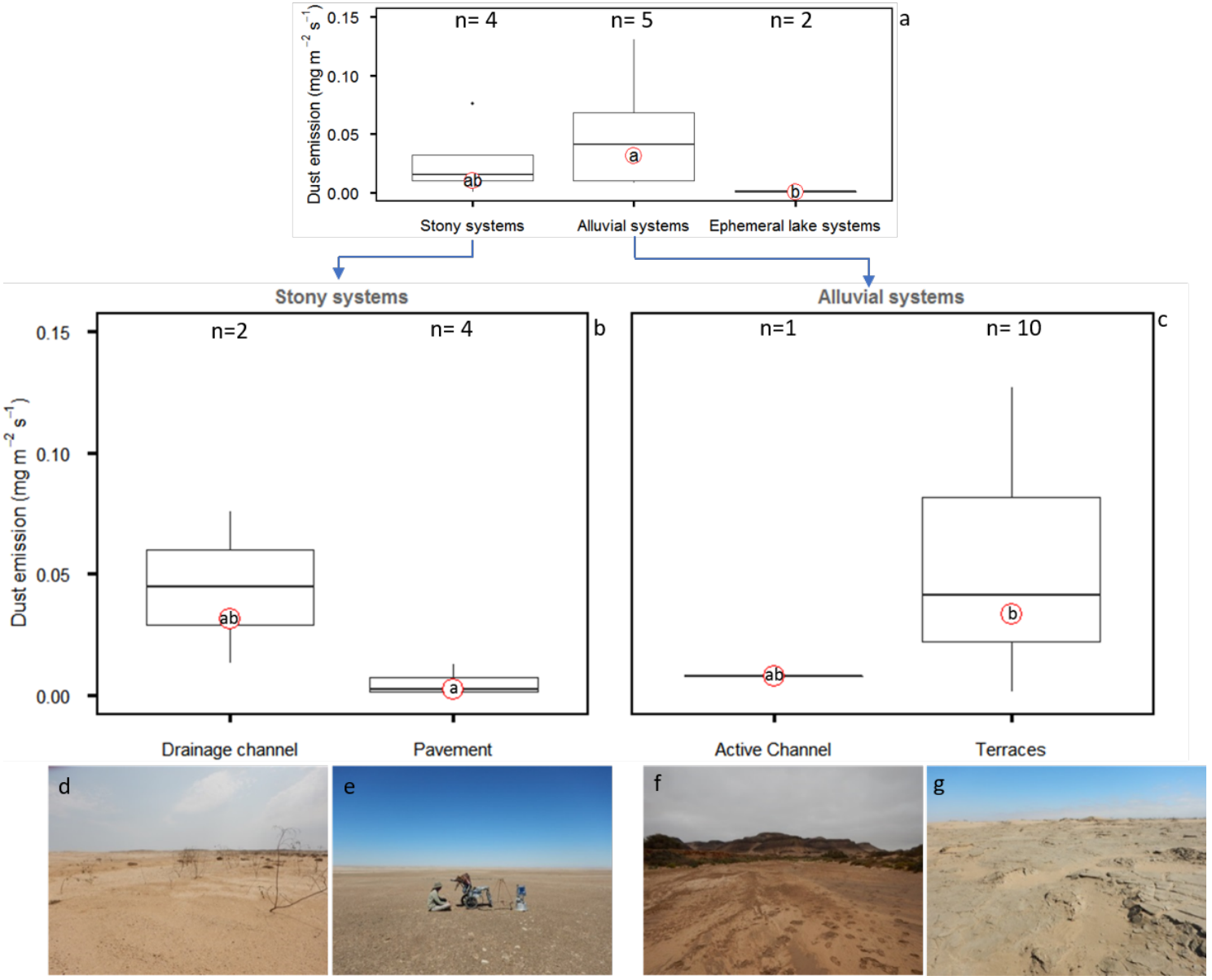
Dust emission (mg m $^{-2}$ s $^{-1}$)
0.15
0.10
0.05
0.00
n= 4
n= 5
n= 2
a
ab
a
b
Stony systems
Alluvial systems
Ephemeral lake systems
Stony systems
Alluvial systems
n=2
n= 4
b
n=1
n= 10
c
ab
a
ab
b
Drainage channel
Pavement
Active Channel
Terraces
d
e
f
g

487

Figure 4 Dust emission determined from PI-SWERL measurements at landscape scale for stony, alluvial and ephemeral lake systems (a). Stony systems consisted of two landform categories: stone pavements and pavement intersected by ephemeral drainage channels (b). Similarly, alluvial systems contained two landforms: active river channels and floodplain terraces (c). Corresponding photographs of each landform are shown at the bottom (d to g). Circled letters indicate statistical difference determined and are plotted at the geometric mean value for each distribution. River terraces proved to have the highest dust emissions in alluvial systems, while no significant difference was observed between drainage channels and pavement within stony landscapes.

Table 2 Summary statistics for PI-SWERL dust flux measurements at the Landscape, Landform and Surface scale assessments

	n[a]	n[b]	Geometric mean (mg m^{-2} s^{-1})	CI low[c] (mg m^{-2} s^{-1})	CI high[d] (mg m^{-2} s^{-1})	Geo SD (mg m^{-2} s^{-1})	Min[e] (mg m^{-2} s^{-1})	Max[f] (mg m^{-2} s^{-1})
Surfaces (n = 128 individual PI-SWERL measurements)								
Low % gravel	17	17	0.0204	0.0076	0.0566	8.544	0.0005	0.2129
High % gravel	9	9	0.0022	0.0009	0.0052	4.378	0.0004	0.0155
Loose erodible material	25	25	0.3188	0.2143	0.4861	2.898	0.0417	1.854
Crust: no saltators	31	31	0.0046	0.0027	0.0071	4.016	0.0003	0.0704
Crust: med saltators	12	12	0.0855	0.0578	0.1359	2.258	0.0102	0.2097
Crust: high saltators	22	22	0.3418	0.2690	0.4356	1.730	0.1575	0.8649
Salt crust: with and without saltators	12	12	0.0008	0.0002	0.0026	8.146	0.00006	0.0210
Total n	128	128						
Landform (n = 17 PI-SWERL transects)								
Terraces	10	75	0.0651	0.0376	0.1194	2.680	0.0111	0.2191
River channel*	1	9	0.0082	0.0014	0.0491	10.258	0.0009	0.1689
Pavement	4	11	0.0075	0.0010	0.0436	10.416	0.0006	0.1501
Drainage channel	2	13	0.0318	0.01332	0.0759	3.422	0.0133	0.0758
Total n	17	108[g]						
Landscape (n = 12 landforms)								
Alluvial systems	5	84	0.0379	0.0179	0.0881	2.848	0.0082	0.1310
Stony systems	4	24	0.0102	0.0019	0.0726	7.468	0.0006	0.0759
Aeolian systems*	1	3	0.0640	0.0406	0.1001	1.199	0.0534	0.0767
Ephemeral lake systems	2	17	0.0022	0.0005	0.0094	7.479	0.0005	0.0094
Total n	12	128						

[a.] Sample size n after aggregation of individual PI-SWERL measurements to relevant scale of enquiry
[b.] Sample size n using individual PI-SWERL measurements
[c.] 95% confidence interval below the mean [d] 95% confidence interval above the mean
[e] Minimum emissions from unit/surface
[f] Maximum emissions from unit/surface
[g.] Landform assessment does not include Aeolian systems (n=3) and Lake systems (n=17)
*Summary statistics calculated with individual measurements as insufficient n at aggregated level (n=1)

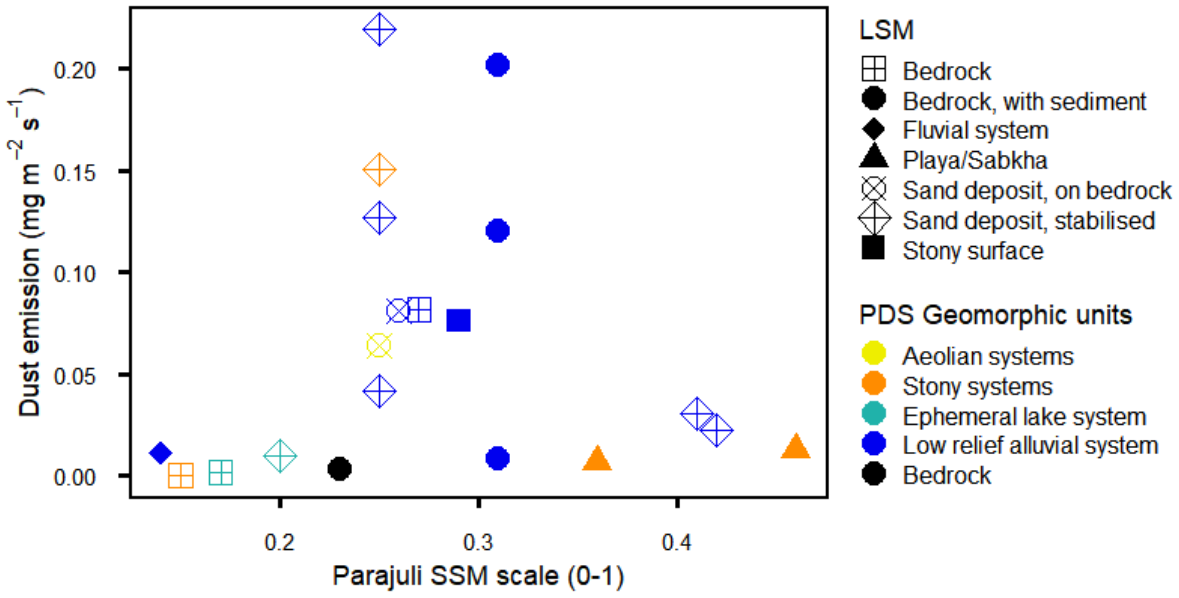

512

513

514 **Figure 5 Dust emission flux measured with the PI-SWERL compared to the SSM (Sediment**
515 **Supply Map) value for each of the transect sample sites. The legend also indicates the land**
516 **surface classification according to the LSM (Land Surface Map) (by symbol shape), and**
517 **secondly, as mapped using the land surface classes proposed by the PDS (Preferential Dust**
518 **Scheme) by symbol color.**

519

4.4 Predictors of emission rate as determined by Boosted Regression Tree analysis

The BRT model produced the following variables as the most important predictors for dust emitted during the PI-SWERL runs: gravel cover (%), moisture content (%), kurtosis, very coarse silt fraction (%), very fine sand (%), fine sand (%), compressive strength (kg m^{-2}), Ca (%), Mg (%) and S (%). The relative contribution of each variable to the model is given as a % and the partial dependence plots (Figure 6) provide the relationship between the variables and the measured dust flux when all other variables are held constant. The trend in the plots is informative, rather than actual values, with increasing partial dependence values indicating increased dust emission and vice versa. A sudden change indicates a critical threshold at which the dust emission flux changes. Taken together, the significant predictor variables identified with the BRT explain 70.8% of the deviance in the dust flux measured with the PI-SWERL.

Based on the BRT analysis, soils layers with a content of very coarse silt above 5% and a very fine to fine sand content between 10 and 20%, resulting in a platykurtic particle size distribution, should indicate areas with potentially increased emission potential. In addition, the density of gravel cover results in an increase in roughness and bed armoring which appears to exert a significant influence in reducing emission potential when gravel content is 15% or above. Moisture has long been regarded as a primary control on dust emission (e.g. Ishizuka et al., 2005; McKenna-Neuman & Nickling, 1989; Munkhtsetseg et al., 2016) and emerges as a primary predictor. Calcium and magnesium were also identified as important elements potentially due to the effect that carbonate minerals have on the erodibility of a crusted soil, with some suggesting these minerals will act to strengthen crusts by acting as a binding agent (Gillette et al., 1982) and others contending that calcite offers very little resistance to abrasion (Pye and Tsoar, 1990). Our data seem to support a reduction in dust flux with increasing Ca and Mg content.

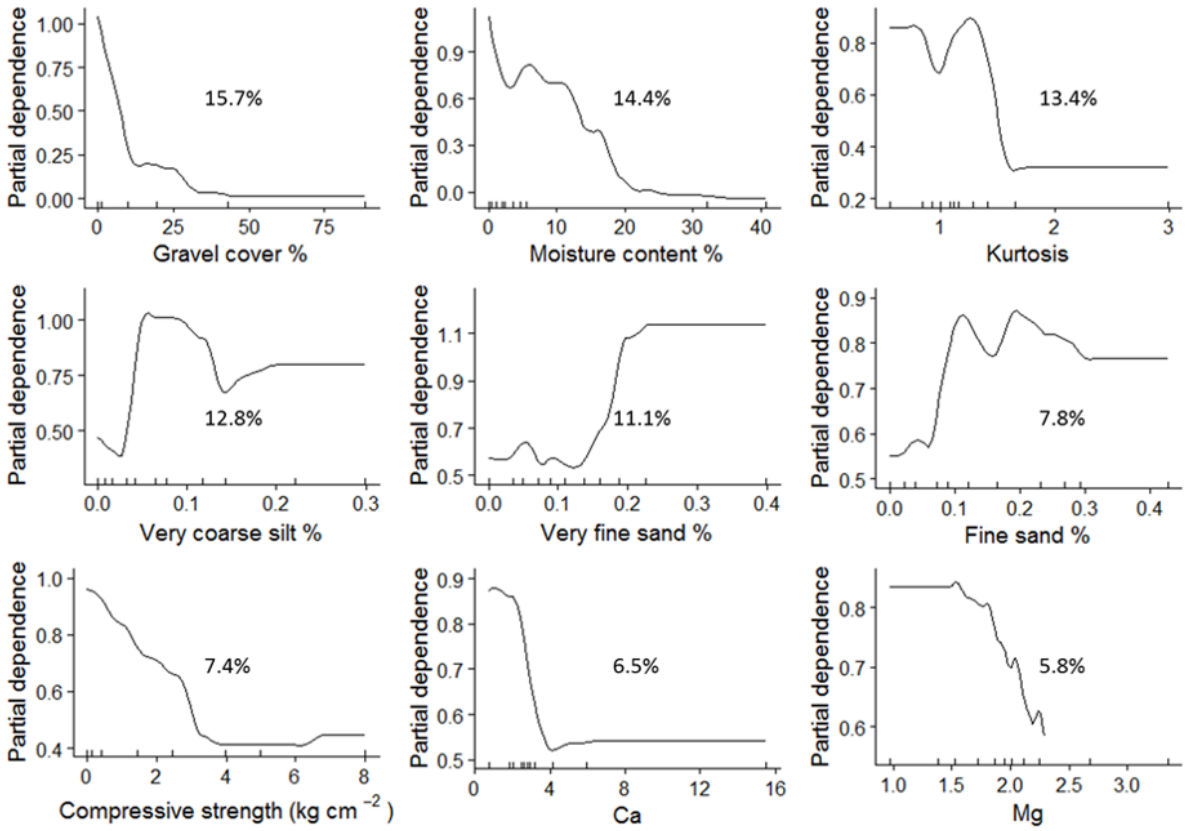

550

551 **Figure 6 Partial dependence plots depicting the relationship between dust emission and each**
552 **significant surface variable. The trend rather than the actual values is the important feature in**
553 **each plot. Increasing partial dependence values indicates an increase in dust flux and decreasing**
554 **values the opposite. Percentage values reported at the centre of each panel are the relative**
555 **influence of variables for predicting dust emission.**

556

5 Discussion

The acquisition of landform scale dust source data achieved here allows for the evaluation of the PDS and LSM classification schemes. It also allows an assessment of the newly generated landscape-scale SSM product to characterise dust emission potential within the Namib Desert. The Namib represents an ideal region for such an investigation as it is host to a variety of actively emitting surfaces (Vickery et al., 2013; von Holdt et al., 2017). Classifying the dust source points identified with Landsat by von Holdt et al. (2017) according to the PDS at a landscape scale indicates that dust emission from the Namib Desert is spatially highly concentrated, with relatively high densities of plumes found to originate from the alluvial systems (0.4 points km^2) and dry lakes (0.9 points km^{-2}) compared to aeolian (0.001 points km^2) and stony systems (0.011 points km^2) (Figure 2). Mapping the land surface classes of the Namib Desert according to the PDS at landscape scale shows the limited extent of ephemeral lakes (playas and sabkhas) as dust producing areas (2% of the total study area) which reflects the hotspot nature of dust production in these landscapes noted by Gillette (1999).

The advantage of the PDS map is that it can represent the landscape in detail because of the high-resolution, quality controlled geomorphic attribution of the surface that comes from user-defined mapping. The disadvantage of this scheme is that it requires certain inputs to map the landscape, which are not consistently available for all areas, and its critical requirement for land surface classes or geomorphic units to be identified and created, which is prone to subjectivity. The PDS mapping has only been performed for limited areas (e.g. Baddock et al., 2011; Bullard et al. (2011); Lee et al., 2012) and creating a global PDS map remains a challenge. Using the LSM developed by Parajuli et al (2014) to map the study area results in an overestimation of the dust emitting alluvial and dry lake areas (Figure 1 c). This is due to the misclassification of several land surface classes which occurs as a result of a supervised technique with training classes based on the spectral signature of the MENA (Middle East and Africa) region (Parajuli & Zender, 2017). The difficulties of such an automated approach demonstrates the problems of attempting to create a global geomorphology classification map. Even though a global land surface classification or geomorphology map would provide a valuable input to the representation of dust emission, the use of region specific training classes should be exercised with caution, especially when based on spectral data. A further limitation of a qualitative geomorphic mapping scheme, such as the PDS and LSM, involves the representation of a quantified dust emission potential.

589 A quantified representation of the dust emission potential for different land surface classes at
590 a landscape-scale in raster format is necessary to incorporate these schemes into dust cycle
591 models. For the PDS this has not been achieved and each class is assigned a qualitative
592 categorical indicator based on inferred emission potential, although the scheme has been tested
593 against long-term frequency of dust observation in the Chihuahuan Desert (Baddock et al.,
594 2016). With PDS, emission information is required to discriminate between relative emission
595 potential from different regions that act as dust sources. A quantification of the dust emission
596 potential of the LSM land cover categories was attempted by Parajuli et al. (2014) using a
597 correlation between ERA-Interim wind speed at 10 m height and MODIS deep blue AOD at
598 550 nm. The authors point out that a disadvantage of this approach is the difference in scale
599 between the high-resolution land cover map and the coarser (1° × 1°) correlation map which
600 results in a disconnect between land cover and the emission potential assigned to them. The
601 location of the major Namib Desert dust sources in the low-relief terminal stages of the rivers
602 and coastal lake systems (pans and sabkhas) poses difficulties for identification of these sources
603 based on techniques relying on aerosol loadings Furthermore, the use of atmospheric aerosol
604 loading estimates, such as MODIS AOD or TOMS AI to locate dust sources in the Namib
605 Desert may well have specific limitations. For example, detection of dust over bright desert
606 surfaces using ultraviolet, visible or thermal infrared wavelengths can be problematic (Baddock
607 et al., 2009; Hsu et al., 2004; Resane et al., 2004). In contrast, MODIS Deep Blue (MODIS
608 DB) can only be retrieved over bright surfaces and is of limited use over dark ocean surfaces,
609 while TOMS AI is known to not detect dust from the Namib Desert at low altitude near the
610 coast (Mahowald & Dufresne, 2004). A consequence of this suite of limitations is that creation
611 of an erodibility map derived from supervised classes established in a different region together
612 with reliance on emission quantification from satellite retrieved aerosol loadings would likely
613 result in a number of dust producing areas, such as the Namib Desert, being underestimated.
614 Field based studies that include PI-SWERL emission measurements from intensely-sampled
615 regions can provide relative dust fluxes, as well as indications of variability, that can serve as
616 inputs for the quantification of dust potential schemes such as the PDS and LSM (Table 2).

617 The recently proposed SSM provides a global landscape-scale erodibility map with a
618 quantification of dust emission potential by combining a physical and empirical approach. The
619 incorporation of upstream drainage area represents the supply of sediment and the surface
620 reflectance represents the different sediment characteristics of the land surface types (Parajuli
621 & Zender, 2017). The SSM dust potential scheme is a novel attempt to provide a global

representation of erodibility at the landscape-scale, elegantly tuned to a maximum potential represented by the Bodélé Depression in Chad. However, the landform-scale assessment of the SSM presented here highlights that there are potential shortcomings in this erodibility map. The dust source points identified with Landsat analysis indicates that most of the dust hot spots in this area are situated in the terminal stages of the rivers as they near the Atlantic Ocean and the coastal sabkhas (Figure 1, and see von Holdt et al., 2017). The SSM classification however identifies areas with high emission potential significantly upstream of the confirmed dust sources, including areas covering large areas of stony systems adjacent to alluvial and dry lake sources (Figure 1e). Furthermore, rivers that are not significant dust sources, such as the Swakop River (marked W in Figure 1 e) are identified as highly emissive in the SSM. The relative absence of dust emission from the Swakop River is probably due to the incised nature of this river combined with less topographic channelling of the high magnitude north-easterly Bergwind compared to other more emissive rivers such as the Kuiseb River. In addition, many parts of the Namib ephemeral rivers hold lush vegetation sustained by groundwater so that significant vegetative roughness make sediments unavailable for entrainment (von Holdt & Eckardt, 2018). As a result, the raised emission potential associated with enhanced alluvial sediment supply is likely to be overestimated in the SSM. It follows that, in addition to the preferential dust source areas identified by the classifications as applied to the Namib, the influences of vegetation and topographic channelling would need to be adequately parameterised in any dust model operating at this regional scale.

The assessment of SSM values for dust emission source points identified with Landsat and measured for dust flux with the PI-SWERL indicate that the SSM scheme does not always agree with the dust emission analysis presented here. The mean SSM value for the location of all Landsat dust emission source points of 0.245 is just under half the maximum emission value of 0.519 for the Namib region. Only 4.7% of the 2289 dust source points were classified in the most emissive category >0.4. Although the dust source points identified by Landsat do not provide a continuous numerical quantification of the dust emission potential, this point source inventory does identify areas which should be assigned values of high emissivity similar to the method used by Parajuli & Zender (2017) in assigning a maximum value of 1 to the Bodélé Depression. In addition, there is no clear relationship between the SSM emission values and PI-SWERL emission results (Figure 5). Sites exhibiting high emission rates were not necessarily classified as highly emissive according to the SSM. The most emissive site as measured with the PI-SWERL (geometric mean dust flux: 0.2191 mg m^{-2} s^{-1}) is situated on the

alluvial system terraces and have an SSM value of 0.25 and classified as stabilised sand deposit by LSM. The highest SSM value (0.46) associated with the PI-SWERL runs was situated within the stony system with a geometric mean dust flux of 0.0127 mg m^{-2} s^{-1}, but classified as lake system by the LSM due to the high surface reflectance of the quartz stone pavement . In this context, the PI-SWERL provides a quantification of dust emission by which to compare the dust emission potential from different surface types or landform- and landscape-scale geomorphic units and offers a means to validate dust-emission schemes. Dust emission is highly variable as indicated by the PI-SWERL dust flux measurements from the different surfaces (Figure 3 Table 2). The small-scale variability that exists at sub-landform scale has been seen to exert a clear effect on dust emission, so adequate representation of this variability remains an important yet persistently challenging research goal. The combination of the Landsat dust point source and PI-SWERL dust flux measurements at landform and sub-landform scale can make contributions as input and validation for landscape-scale dust-emission schemes.

The PI-SWERL potentially provides a standardised quantification of surface dust emissions across different dust-producing regions, however comparison between different studies and regions would require consistency in measured parameters and landform categories. We offer an attempt at such a comparison by relating our results to Sweeney et al. (2011) from the Mojave Desert, USA (referred to from hereon as SW2011), which shows agreement between some of the measured surfaces, landforms and landscapes (Figure 7). An important legitimacy to this comparison is that SW2011 tested at the same friction velocity (u_* = 0.56m s^{-1}) as our study. The pavements in the stony systems and lakes systems compare well, whereas the aeolian systems have good agreement between the geometric means and lower confidence interval, but SW2011 report a much larger upper confidence interval. This is potentially due to SW2011 consisting of many more replicates for this landform category (30 versus 3 for the present study) and the dunes from the Mojave study being potentially situated adjacent to a large pan. In turn, the dunes tested as part of the Namib study were situated near an ephemeral river (Figure 1 a, approximately 1km south of Kuiseb delta), which would introduce potentially finer material than dunes situated farther from such a source. This comparison illustrates the importance of site-specific controls in accounting for the degree of inherent emission variability for a given surface type and indicates their importance for understanding dust fluxes as quantified from field testing in different locations. Aeolian systems can cover large areas and their emission potential can vary greatly depending on factors such as dune type,

mineralogy and age (Bristow & Moller, 2018; Bullard et al., 2011). Dunes rarely produce distinct point sources visible on satellite imagery (as is the case for this Namib dataset, Figure 2) but have the potential to be contributing sources of dust, albeit at low volumes, due to their areal extent. The dust emission potential of the Sand Seas of the Namib requires further investigation. Furthermore, what was classified as a stony system with drainage in this study probably most closely corresponds with a wash as per SW2011, which SW2011 determined to be considerably more emissive (SW2011 Wash geometric mean: 0.3915 mg m^{-2} s^{-1} vs geometric mean of stony system with drainage in present study: 0.0102 mg m^{-2} s^{-1}). An important difference may well be down to fact that the stony systems with drainage classified as a landform in the Namib study typically did not feature a supply of sand available for saltation at the sites we tested, thereby they corresponded to a gravel-covered surface, rather than an LEM-dominated one (Figure 3). The LEM surface category from this study and the wash (Landform) from SW2011 were the two most emissive categories and represent a maximum emission value for the two studies. Despite LEM representing a surface type and wash a landform type, the upper limit of emission shows good agreement and again illustrates the importance of landform and surface interpretation.

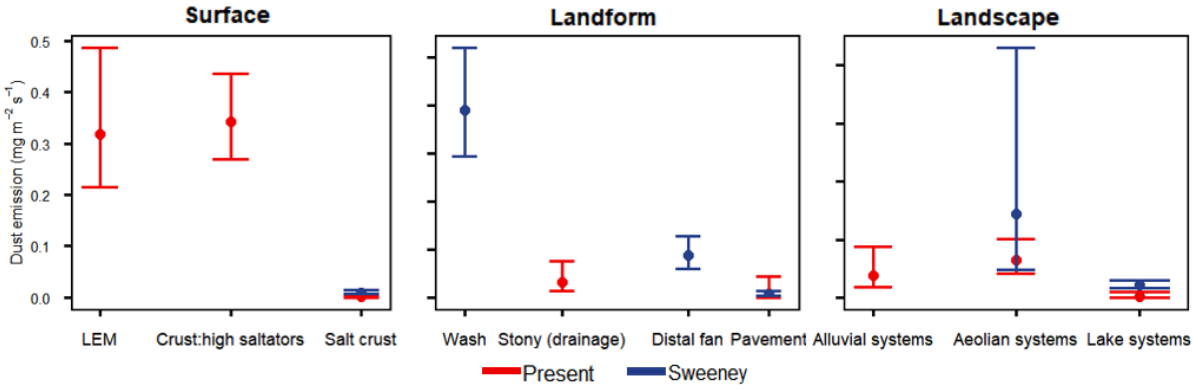

Figure 7 Comparison between the present study (red lines) and results from Sweeney et al. (2011) (blue lines) for the Mojave Desert, USA (both studies tested at u_* = 0.56m s^{-1}). Selected surfaces, landforms and landscape classes from both studies were chosen for comparison. The stone pavement and dry lakes (pans) show good agreement. Correspondence is shown between the two studies for the categories with maximum emission values (wash for Sweeney et al., 2011 and LEM surface type for present study).

712 The PI-SWERL measurements also can be used to assess sufficiency of sample size for
713 different scales of analysis, both for the current study and as a guide for future efforts. Because
714 our approach aggregates individual measurements with increasing scale of analysis, sample
715 sizes are reduced (from n=128 for individual PI-SWERL to n=12 for landscape systems, Table
716 1). This, in turn, affects the confidence intervals for each scale of analysis, with results
717 indicating that the current sampling effort may be insufficient to resolve significant differences
718 for some categories at the landform and landscape levels (Figure S4). Similarly, power analyses
719 demonstrate that larger sample sizes may be needed than the current effort for all scales of
720 analysis (Figure S5); requisite sample sizes are 60 per surface type, 22 transects per landform,
721 and 12 landforms per landscape. However, analysis of confidence intervals (which
722 demonstrates the impact of sample variance and sample size on uncertainty of the mean) are
723 generally preferred to a post hoc power analysis (Hoening & Heisey, 2001; Goodman & Berlin,
724 1994). Regardless, the above results indicate that, despite the extensive sampling effort
725 involved in our study (128 measurements), larger sample sizes may be needed in future work,
726 particularly at landform and landscape scales due to their large confidence intervals (Figure
727 S4).

728 Another potential approach to develop and improve dust-emission schemes with high-
729 resolution/fine-scale PI-SWERL data is to assess the factors that control the erodibility of the
730 surfaces. This is especially useful for factors that are represented in datasets that are available
731 globally, such as particle size and moisture data. The BRT analysis highlighted the significant
732 variables for PM_{10} dust flux measured with the PI-SWERL at a set friction velocity. The partial
733 dependency plots additionally highlight information on critical thresholds where dust emission
734 takes place or ceases on different surfaces (Figure 6). An important consideration for such
735 analysis is the choice of variables and the method of measurement. For example, the need to
736 sample moisture close to the surface meant that moisture was determined only as a relative
737 estimate at our test sites, not a quantified measure throughout the soil column. A more accurate
738 reflection of the moisture content would have been obtained by a gravimetric determination of
739 the top 1 cm of the soil surface, which would provide an indication of the soil moisture (%)
740 and its influence on the erosion threshold (u_{*t}). Furthermore, our approach of sampling soil
741 moisture in the upper 2 cm of the surface, rather than directly at the surface may have reduced
742 the performance of the BRT, particularly for samples taken from lake system playas and
743 sabkhas. When those data points are excluded, a critical moisture threshold of 2% is obtained
744 for the tested friction velocity of approximately 0.58 m s^{-1}. This moisture content threshold is

similar to the value of 0.02 g g^{-1} soil moisture obtained by Munkhtsetseg et al. (2016) above which they observed that dust emission became significantly depressed.

Of further critical importance here are the environmental conditions at the time of surface testing. The long-term Landsat record established that the ephemeral lakes are highly emissive (Figure 2), in accordance with many dust sources (e.g. Gill, 1996; Reynolds et al., 2009; Bullard et al., 2008; Ginoux et al., 2012), but their emissivity was relatively low during the PI-SWERL testing due to the prevailing elevated humid conditions in proximity to the coast at the time of PI-SWERL testing, as well as the hygroscopic saline surfaces and periodic shallow water nature which can create wet playas (Reynolds et al., 2009; Sweeney et al., 2016). This also raises an important issue regarding dust emission not captured with remote sensing. The ephemeral lakes of the Namib are highly emissive during the Bergwind events that coincide with the overpass of the polar-orbiting satellites (MODIS and Landsat). However, the conditions are dominated by high relative humidity along the coast which also prevailed at the time of testing. The effect of such environmental controls is underscored by the fact that during high relative humidity along the coast, MODIS and Landsat indicate the alluvial flood terraces remained emissive, whereas the coastal-adjacent ephemeral lakes were non-emissive. As a result, we could be over-estimating the emissions form these lakes. Relative humidity should be a standard measurement that has to be recorded at the time of PI-SWERL testing. The BRT analysis should also be extended by testing at different friction velocities to determine the threshold at which emission is initiated. Furthermore, by identifying the significant variables, a set of surface characterisation tests can be developed that should be included when measuring emission potential. Combining a standard set of surface characterisation tests and dust flux measurements from different well-known hot spots around the world can be used to substantially improve dust-emission schemes.

6 Conclusion

This study provides a ground-based assessment of recently proposed dust-emission mapping schemes that highlights limitations in our ability to represent dust emission potential at large scales. The novel combination of a high resolution (Landsat-derived), sub-landscape scale inventory of actively eroding parts of the Namib Desert together with the ground-based measurement of dust emission rates using PI-SWERL at known point sources allows a qualitative and quantitative evaluation of two approaches to classify emission potential. Our findings demonstrate that point measurements of emission, coupled with characterization of

surface properties (soil moisture, degree of crusting, particle size and elemental composition as proxy for mineralogy) at the time of testing, can provide valuable information for assessing and potentially improving larger-scale schemes for predicting dust emission potential.

The combination of a physical and empirical approach such as that used to create the Sediment Supply Map (SSM) (Parajuli & Zender, 2017) is useful at capturing the relevant factors for surface erodibility and emission potential based on globally-applicable data sets. The SSM represents sediment supply on the basis of drainage area (a proxy for hydrology) and surface reflectance, but in the Namib, alluvial systems, seen here to be areas of potentially high emission, are mapped by SSM as lying significantly upstream and over a greater extent compared to the distribution of active dust source points identified via remote sensing. In the case of emission potential determined from user-defined geomorphic mapping such as that offered by PDS (Bullard et al., 2011), challenges include determining the inputs and effort required to apply the scheme across a region, as well as variability of emission within a given class. Our sub-landform measurements indicate that variability of emission rates remains an inherent problem for each of the emission classification schemes examined in our study. However, results such as ours can be used to further parameterize the range of emission fluxes for land surface classes in dust-cycle models. The current study reveals how PI-SWERL dust-emission measurements provide a relative quantification of landform emissivity which can provide modelers with the range of emission fluxes for given geomorphic classes in emission potential mapping schemes.

Use of a Boosted Regression Tree (BRT) model identifies significant surface characteristics and critical thresholds related to dust emission that can be used to inform dust models. The BRT analysis for the Namib Desert highlighted the importance of soil moisture content, crust strength and particle size kurtosis, with critical thresholds for dust emission additionally dependent on gravel density and the presence of sand and silt. Our approach provides a framework for obtaining site-specific values in other dust-source regions and may help to standardize datasets for global dust emission modeling. A standardised set of surface characterisation tests combined with dust flux measurements would offer regional and global datasets of relative emission potential and thereby provide utility for developing dust emission schemes toward improved dust emission modeling.

807 **Acknowledgements**

808 This research was funded by the National Research Foundation in South Africa as part of
809 research project number: UID 89120. The authors would like to thank Suzette Heath, Peter
810 Bridgeford, Jo Nield and Ruusa Gottlieb for assistance in the field. Thank you to Michael
811 Cramer for advice on running the BRT and to Martin Hipondoka for his contribution to this
812 study. Thank you to Sagar Parajuli for making the LSM and SSM datasets available to us. We
813 thank the Ministry of Environment and Tourism for their support and assistance for the duration
814 of this research. This research was conducted under MET permit number 2076/2015. The
815 authors are grateful for helpful remarks by Joel Sankey, Mark Sweeney and the other
816 anonymous reviewer, as well as the valuable contributions of Associate Editor Amy East, and
817 Editor John M. Buffington. The data used in this manuscript is available on Figshare at
818 **https://doi.org/10.25375/uct.7454210.v2**.

819

820 **References**

821 Ashpole, I. & Washington, R., 2013. A new high-resolution central and western Saharan
822 summertime dust source map from automated satellite dust plume tracking. *Journal of*
823 *Geophysical Research: Atmospheres*, *118*(13), pp.6981-6995.

824 Bacon, S.N., McDonald, E. V., Amit, R., Enzel, Y. & Crouvi, O. 2011. Total suspended
825 particulate matter emissions at high friction velocities from desert landforms. *Journal*
826 *of Geophysical Research: Earth Surface*. 116(3):1–17. DOI: 10.1029/2011JF001965.

827 Baddock, M.C., Bullard, J.E. & Bryant, R.G., 2009. Dust source identification using MODIS:
828 a comparison of techniques applied to the Lake Eyre Basin, Australia. *Remote Sensing*
829 *of Environment*, *113*(7), pp.1511-1528.

830 Baddock, M.C., Ginoux, P., Bullard, J.E. and Gill, T.E. (2016), Do MODIS-defined dust
831 sources have a geomorphological signature? *Geophysical Research Letters*.
832 43(6):2606–2613. DOI: 10.1002/2015GL067327.

833 Belnap, J. & Gillette, D.A., 1998. Vulnerability of desert biological soil crusts to wind
834 erosion: the influences of crust development, soil texture, and disturbance. *Journal of*
835 *Arid Environments*, *39*(2), pp.133-142.

836 Blott, S.J. & Pye, K., 2001. GRADISTAT: a grain size distribution and statistics package for
837 the analysis of unconsolidated sediments. *Earth Surface Processes and*
838 *Landforms*, *26*(11), pp.1237-1248.

839 Bristow, C.S. and Moller, T.H., 2018. Dust Production by Abrasion of Eolian Basalt Sands:
840 Analogue for Martian Dust. *Journal of Geophysical Research: Planets*, *123*(10),
841 pp.2713-2731.

842 Bryant, R.G., Bigg, G.R., Mahowald, N.M., Eckardt, F.D. & Ross, S.G. 2007. Dust emission
843 response to climate in southern Africa. *Journal of Geophysical Research*. 112(D9):1–
844 17. DOI: 10.1029/2005JD007025.

845 Buck, B.J., King, J. and Etyemezian, V., 2011. Effects of salt mineralogy on dust emissions,
846 Salton Sea, California. Soil Science Society of America Journal, *75*(5), 1971-1985.

847 Bullard, J.E., Harrison, S.P., Baddock, M.C., Drake, N., Gill, T.E., McTainsh, G. & Sun, Y.,
848 2011. Preferential dust sources: A geomorphological classification designed for use in

global dust-cycle models. *Journal of Geophysical Research: Earth Surface*, *116*(F4). DOI**:** 10.1029/2011JF002061

Bullard, J., Baddock, M., McTainsh, G. & Leys, J. 2008. Sub-basin scale dust source geomorphology detected using MODIS. *Geophys. Res. Lett.*. 35:1–6. DOI: 10.1029/2008GL033928.

Bullard, J.E., Mctainsh, G.H. & Pudmenzky, C. 2004. Aeolian abrasion and modes of fine particle production from natural red dune sands : an experimental study. *Sedimentology*. 51:1103–1125. DOI: 10.1111/j.1365-3091.2004.00662.x.

Cornelis, W.M., Gabriels, D., Hartmann, R., 2004. A conceptual model to predict the deflation threshold shear velocity as affected by near-surface soil water: II. Calibration and validation. Soil Science Society of America Journal 68, 1162–1168.

Crouvi, O., Amit, R., Enzel, Y., Porat, N. & Sandler, A. 2008. Sand dunes as a major proximal dust source for late Pleistocene loess in the Negev Desert , Israel. *Quaternary Research*. 70:275–282. DOI: 10.1016/j.yqres.2008.04.011.

Dansie, A.P., Thomas, D.S.G., Wiggs, G.F.S. and Munkittrick, K.R. 2018 Spatial variability of ocean fertilising nutrients in the dust-emitting ephemeral river catchments of Namibia. *Earth surface processes and landforms*, 43: 563-578.

Eckardt, F.D. and Kuring, N. 2005. SeaWiFS identifies dust sources in the Namib Desert. *International journal of remote sensing*, *26*(19), pp.4159-4167.

Eitel, B., Blümel, W.D., Hüser, K. and Mauz, B., 2001. Dust and loessic alluvial deposits in Northwestern Namibia (Damaraland, Kaokoveld): sedimentology and palaeoclimatic evidence based on luminescence data. Quaternary International, 76, pp.57-65.

Elith, J., Leathwick, J.R. & Hastie, T. 2008. A working guide to boosted regression trees. *Journal of Animal Ecology*. 77(4):802–813. DOI: 10.1111/j.1365-2656.2008.01390.x.

Etyemezian, V., Nikolich, G., Ahonen, S., Pitchford, M., Sweeney, M., Purcell, R., Gillies, J. & Kuhns, H. 2007. The Portable In Situ Wind Erosion Laboratory (PI-SWERL): A new method to measure PM10 windblown dust properties and potential for emissions. Atmospheric Environment. 41(18):3789–3796. DOI: 10.1016/j.atmosenv.2007.01.018.

878 Gill, T. E. (1996), Eolian sediments generated by anthropogenic disturbance of playas:
879 Human impacts on the geomorphic system and geomorphic impacts on the human
880 system, Geomorphology, 17, 207–228, doi:10.1016/0169-555X(95)00104-D.

881 Gillette, D.A. Adams, J., Muhs, D. & Kihl, R., 1982. Threshold friction velocities and rupture
882 moduli for crusted desert soils for the input of soil particles into the air. *Journal of*
883 *Geophysical Research*, 87(C11), p 9003. Available at:
884 http://doi.wiley.com/10.1029/JC087iC11p09003.

885 Gillette, D. A., 1999 A qualitative geophysical explanation for "hot spot" dust emitting
886 source regions, *Contrib. Atmos. Phys.*, **72**, 67– 77.

887 Gillies, J.A., Nickling, W.G. and King, J., 2006. Aeolian sediment transport through large
888 patches of roughness in the atmospheric inertial sublayer. *Journal of Geophysical*
889 *Research: Earth Surface*, *111*(F2).

890 Gillies, J. A. (2013), Fundamentals of aeolian sediment transport: Dust emissions and
891 transport—Near surface, in *Treatise on Geomorphology*, edited by J. Shroder and N.
892 Lancaster, pp. 43–63, Academic Press, San Diego, Calif.

893 Ginoux, P., Chin, M., Tegen, I., Prospero, J.M., Holben, B., Dubovik, O. and Lin, S.J., 2001.
894 Sources and distributions of dust aerosols simulated with the GOCART
895 model. Journal of Geophysical Research: Atmospheres, 106(D17), pp.20255-20273.

896 Ginoux, P., Prospero, J.M., Gill, T.E., Hsu, N.C. & Zhao, M. 2012. Global-Scale Attribution
897 of Anthropogenic and Natural Dust Sources and Their Emission Rates Based on
898 Modis Deep Blue Aerosol Products. 1–36. DOI: 10.1029/2012RG000388.

899 Goodman, S.N. and Berlin, J.A., 1994. The use of predicted confidence intervals when
900 planning experiments and the misuse of power when interpreting results. *Annals of*
901 *internal medicine*, *121*(3), pp.200-206.

902 Goossens, D. & Buck, B., 2009. Dust emission by off-road driving: Experiments on 17 arid
903 soil types, Nevada, USA. *Geomorphology*, *107*(3), pp.118-138.

904 Goudie, A. and Viles, H., 2015. Climate. In *Landscapes and Landforms of Namibia* (pp. 37-
905 46). Springer Netherlands.

906 Grini, A., Myhre, G., Zender, C.S. & Isaksen, I.S., 2005. Model simulations of dust sources
907 and transport in the global atmosphere: Effects of soil erodibility and wind speed
908 variability. Journal of Geophysical Research: Atmospheres, 110(D2).

909 Haustein, K., Washington, R., King, J., Wiggs, G., Thomas, D. & Menut, L., 2015. Testing
910 the performance of state-of-the-art dust-emission schemes using DO4Models field
911 data. *Geosci Model Dev Discuss*, *7*, pp.5739-5789.

912 Hijmans, R.J., Phillips, S., Leathwick, J. and Elith, J., 2016. dismo: species distribution
913 modeling.–R package ver. 1.0-15.

914 Hoenig, J.M. and Heisey, D.M., 2001. The abuse of power: the pervasive fallacy of power
915 calculations for data analysis. *The American Statistician*, *55*(1), pp.19-24.

916 Hsu, N.C., Tsay, S.C., King, M.D. and Herman, J.R., 2004. Aerosol properties over bright-
917 reflecting source regions. *IEEE Transactions on Geoscience and Remote*
918 *Sensing*, *42*(3), pp.557-569.

919 Huang, J., Ge, J. & Weng, F. 2007. Detection of Asia dust storms using multisensor satellite
920 measurements. Remote Sensing of Environment. 110(2):186–191. DOI:
921 10.1016/j.rse.2007.02.022.

922 Ishizuka, M., Mikami, M., Yamada, Y., Zeng, F. and Gao, W., 2005. An observational study
923 of soil moisture effects on wind erosion at a gobi site in the Taklimakan Desert.
924 *Journal of Geophysical Research: Atmospheres*, *110*(D18).

925 Jacobson, P. J., Jacobson, K. N., & Seely, M. K. 1995. *Ephemeral rivers and their*
926 *catchments: sustaining people and development in western Namibia*. Desert Research
927 Foundation of Namibia.

928 King, J., Etyemezian, V., Sweeney, M., Buck, B.J. & Nikolich, G. 2011. Dust emission
929 variability at the Salton Sea, California, USA. Aeolian Research. 3(1):67–79. DOI:
930 10.1016/j.aeolia.2011.03.005.

931 Lee, J. A., Gill, T. E., Mulligan, K. R., Dominguez Acosta, M., Perez, A. E., 2009. Land
932 use/land cover and point sources of the 15 December 2003 dust storm in southwestern
933 North America. Geomorphology, 105(December 2003), 18–27.

934 Lee, J. A., Baddock, M.C., Mbuh, M.J. & Gill, T.E. 2012. Geomorphic and land cover
935 characteristics of aeolian dust sources in West Texas and eastern New Mexico, USA.
936 Aeolian Research. 3(4):459–466. DOI: 10.1016/j.aeolia.2011.08.001.

937 Mahowald, N., Luo, C., Corral, J. & Zender, C.S. 2003. Interannual variability in
938 atmospheric mineral aerosols from a 22-year model simulation and observational data.
939 Journal of Geophysical research. 108(D12). DOI: 10.1029/2002JD002821.

940 Mahowald, N.M. and Dufresne, J.L., 2004. Sensitivity of TOMS aerosol index to boundary
941 layer height: Implications for detection of mineral aerosol sources. *Geophysical*
942 *Research Letters*, *31*(3).

943 Marticorena, B. and Bergametti, G., 1995. Modeling the atmospheric dust cycle: 1. Design of
944 a soil-derived dust emission scheme. *Journal of Geophysical Research:*
945 *Atmospheres*, *100*(D8), pp.16415-16430.

946 McFadden, L.D., 2013. Strongly dust-influenced soils and what they tell us about landscape
947 dynamics in vegetated aridlands of the southwestern United States. *Geological Society*
948 *of America Special Papers*, *500*, pp.501-532.

949 McKenna-Neuman, C. & Nickling, W.G., 1989. A theoretical and wind tunnel investigation
950 of the effect of capillary water on the entrainment of sediment by wind. *Canadian*
951 *Journal of Soil Science*, *69*(1), pp.79-96.

952 Neuman, C.M. and Maxwell, C., 2002. Temporal aspects of the abrasion of microphytic
953 crusts under grain impact. *Earth Surface Processes and Landforms: The Journal of*
954 *the British Geomorphological Research Group*, *27*(8), pp.891-908.

955

956 Munkhtsetseg, E., Shinoda, M., Gillies, J.A., Kimura, R., King, J. & Nikolich, G. 2016.
957 Relationships between soil moisture and dust emissions in a bare sandy soil of
958 Mongolia č . Particuology. 28:131–137. DOI: 10.1016/j.partic.2016.03.001.

959 Okin, G.S. and Gillette, D.A., 2001. Distribution of vegetation in wind-dominated
960 landscapes: Implications for wind erosion modeling and landscape processes. *Journal*
961 *of Geophysical Research: Atmospheres*, *106*(D9), pp.9673-9683.

962 O'Loingsigh, T., R.M. Mitchell, S.K. Campbell, N.A. Drake, G.H. McTainsh, N.J. Tapper,
963 and D.L. Dunkerley (2015), Correction of dust event frequency from MODIS Quick-
964 Look imagery using in-situ aerosol measurements over the Lake Eyre Basin,
965 Australia, *Rem. Sens. Environ*., 169, 222-231. doi: 10.1016/j.rse.2015.08.010.

966 Paradis, E. and Schliep, K., 2018. ape 5.0: an environment for modern phylogenetics and
967 evolutionary analyses in R. *Bioinformatics*, *35*(3), pp.526-528.

968 Parajuli, S.P. & Zender, C.S. 2017. Connecting geomorphology to dust emission through
969 high-resolution mapping of global land cover and sediment supply. Aeolian Research.
970 27:47–65. DOI: 10.1016/j.aeolia.2017.06.002.

971 Parajuli, S.P., Yang, Z. & Kocurek, G. 2014. Mapping erodibility in dust source regions
972 based on geomorphology, meteorology, and remote sensing. Journal of Geophysical
973 Research: Earth Surface, 119, DOI: 10.1002/2014JF003095.

974 Pinheiro J, Bates D, DebRoy S, Sarkar D, R Core Team (2018). _nlme: Linear and Nonlinear
975 Mixed Effects Models_. R package version 3.1-137, <URL: https://CRAN.R-projec
976 t.org/package=nlme>.

977 Prospero, J.M., Ginoux, P., Torres, O., Nicholson, S.E. & Gill, T.E., 2002. Environmental
978 characterization of global sources of atmospheric soil dust identified with the Nimbus
979 7 Total Ozone Mapping Spectrometer (TOMS) absorbing aerosol product. *Reviews of*
980 *geophysics*, *40*(1).

981 Pye, K. & Tsoar, H., 1990. Aeolian Sand and Sand Dunes. Unwin Hyman, London. 396p.

982 QGIS Development Team, 2016. QGIS Geographic Information System. Open Source
983 Geospatial Foundation. URL http://qgis.osgeo.org

984 R Core Team (2017). R: A language and environment for statistical computing. R Foundation
985 for Statistical Computing, Vienna, Austria. URL https://www.R-project.org/.
986

987 Raupach, M.R., Gillette, D.A. and Leys, J.F., 1993. The effect of roughness elements on wind
988 erosion threshold. *Journal of Geophysical Research: Atmospheres*, *98*(D2), pp.3023-
989 3029.
990

991 Ravi, S., D'odorico, P., Breshears, D.D., Field, J.P., Goudie, A.S., Huxman, T.E., Li, J., Okin,
992 G.S., Swap, R.J., Thomas, A.D. & Van Pelt, S., 2011. Aeolian processes and the
993 biosphere. *Reviews of Geophysics*, *49*(3)

994 Resane, T., Freiman, T. and Annegarn, H., 2004. The day of the white rain: origin of unusual
995 dust deposition in Johannesburg, South Africa. *South African journal of*
996 *science*, *100*(9), pp.483-487.

997 Reynolds, R.L., Bogle, R., Vogel, J., Goldstein, H. & Yount, J. 2009. Dust emission at
998 Franklin Lake Playa , Mojave Desert (USA): Response to meteorological and
999 hydrologic changes 2005-2008. Natural Resources and Environmental Issues.
1000 15(1):Article 18.

1001 Sankey, J.B., Glenn, N.F., Germino, M.J., Gironella, A.I.N. and Thackray, G.D. (2010),
1002 Relationships of aeolian erosion and deposition with LiDAR-derived landscape
1003 surface roughness following wildfire. *Geomorphology*, *119*(1-2), 135-145.

1004 Sankey, J.B., Eitel, J.U., Glenn, N.F., Germino, M.J. and Vierling, L.A., 2011. Quantifying
1005 relationships of burning, roughness, and potential dust emission with laser altimetry of
1006 soil surfaces at submeter scales. *Geomorphology*, *135*(1-2), pp.181-190.

1007 Schepanski, K., Tegen, I., Laurent, B., Heinold, B. & Macke, A., 2007. A new Saharan dust
1008 source activation frequency map derived from MSG-SEVIRI IR-channels. *Geophys.*
1009 *Res. Lett.*, *34*(18).

1010 Schepanski, K., Tegen, I. and Macke, A., 2012. Comparison of satellite based observations of
1011 Saharan dust source areas. *Remote Sensing of Environment*. 123:90–97. DOI:
1012 10.1016/j.rse.2012.03.019.

1013 Shao, Y.P., Raupach, M.R. and Leys, J.F., 1996. A model for predicting aeolian sand drift
1014 and dust entrainment on scales from paddock to region. *Soil Research*, *34*(3), 309-
1015 342.

1016 Shao, Y., Wyrwoll, K.H., Chappell, A., Huang, J., Lin, Z., McTainsh, G.H., Mikami, M.,
1017 Tanaka, T.Y., Wang, X. and Yoon, S., 2011. Dust cycle: An emerging core theme in
1018 Earth system science. *Aeolian Research*, *2*(4), 181-204.

1019 Shi, M., Yang, Z.L., Stenchikov, G.L., Parajuli, S.P., Tao, W. and Kalenderski, S., 2016.
1020 Quantifying the impacts of landscape heterogeneity and model resolution on dust

emissions in the Arabian Peninsula. *Environmental modelling & software*, *78*, pp.106-119.

Strong C.L., J.E. Bullard, G.H. McTainsh, C. Dubois, and M.C. Baddock (2010), Impact of wildfire on interdune ecology and sediments: an example from the Simpson Desert, Australia, *J. Arid Env.*, 74: 1577-1581. doi:10.1016/j.jaridenv.2010.05.032.

Sweeney, M., Etyemezian, V., Macpherson, T., Nickling, W., Gillies, J., Nikolich, G., and McDonald, E. (2008), Comparison of PI-SWERL with dust emission measurements from a straight-line field wind tunnel. Journal of Geophysical Research: Earth Surface, 113(1), 1–12. doi: 10.1029/2007JF000830

Sweeney, M.R., McDonald, E. V. and Etyemezian, V. (2011), Quantifying dust emissions from desert landforms, eastern Mojave Desert, USA, *Geomorphology*. 135: 21–34. DOI: 10.1016/j.geomorph.2011.07.022.

Sweeney, M.R., McDonald, E.V. and Markley, C.E., (2013), Alluvial sediment or playas: what is the dominant source of sand and silt in desert soil vesicular A horizons, southwest USA. *Journal of Geophysical Research: Earth Surface*, *118*(1), 257-275.

Sweeney, M.R., Zlotnik, V.A., Joeckel, R.M. and Stout, J.E. (2016), Geomorphic and hydrologic controls of dust emissions during drought from Yellow Lake playa, West Texas, USA. DOI: 10.1016/j.jaridenv.2016.05.007.

Taramelli, A., Pasqui, M., Barbour, J., Kirschbaum, D., Bottai, L., Busillo, C., Calastrini, F., Guarnieri, F. and Small, C., 2013. Spatial and temporal dust source variability in northern China identified using advanced remote sensing analysis. *Earth Surface Processes and Landforms*, *38*(8), pp.793-809.

Thomas, D.S., Durcan, J.A., Dansie, A. and Wiggs, G.F., 2017. Holocene fluvial valley fill sources of atmospheric mineral dust in the Skeleton Coast, Namibia. *Earth Surface Processes and Landforms*, *42*(12), pp.1884-1894.

Vickery, K.J., Eckardt, F.D. & Bryant, R.G. 2013. A sub-basin scale dust plume source frequency inventory for southern Africa, 2005-2008. Geophysical Research Letters. 40(19):5274–5279. DOI: 10.1002/grl.50968.

Vickery, K. J. & Eckardt, F. D., 2013. Dust emission controls on the lower Kuiseb River valley, Central Namib. Aeolian Research, 10, 125–133.

1051 von Holdt, J.R., Eckardt, F.D. & Wiggs, G.F.S. 2017. Landsat identifies aeolian dust
1052 emission dynamics at the landform scale. Remote Sensing of Environment. 198:229–
1053 243. DOI: 10.1016/j.rse.2017.06.010.

1054 von Holdt, J.R. and Eckardt, F.D., 2018. Dust activity and surface sediment characteristics of
1055 the dustiest river in southern Africa: the Kuiseb River, Central Namib. *South African*
1056 *Geographical Journal*, *100*(1), pp.104-121.

1057 Wang, X., Lang, L., Hua, T., Wang, H., Zhang, C. & Wang, Z. 2012. Characteristics of the
1058 Gobi desert and their significance for dust emissions in the Ala Shan Plateau (Central
1059 Asia): An experimental study. Journal of Arid Environments. 81:35–46. DOI:
1060 10.1016/j.jaridenv.2012.01.014.

1061 Washington, R., Todd, M., Middleton, N.J. & Goudie, A.S. 2003. Dust-storm source areas
1062 determined by the total ozone monitoring spectrometer and surface observations.
1063 Annals of the Association of American Geographers. 93(2):297–313. DOI:
1064 10.1111/1467-8306.9302003.

1065 Webb, N.P. & Strong, C.L. 2011. Soil erodibility dynamics and its representation for wind
1066 erosion and dust emission models. Aeolian Research. 3(2):165–179.

1067 Wiggs, G.F.S., Baird, A.J. and Atherton, R.J., 2004. The dynamic effects of moisture on the
1068 entrainment and transport of sand by wind. *Geomorphology*, *59*(1-4), pp.13-30.

1069 Zender, C.S., Bian, H. & Newman, D., 2003. Mineral Dust Entrainment and Deposition
1070 (DEAD) model: Description and 1990s dust climatology. Journal of Geophysical
1071 Research: Atmospheres, 108(D14).

1072